2024 IEEE/RSJ International Conference on Intelligent Robots and Systems (IROS)
October 14-18, 2024. Abu Dhabi, UAE

Design and Validation of Flexible Aerial Robotics for Safe Human-Robot Interaction

Fuhua Jia[1,2], Zihao Zheng[1], Cheng'ao Li[1], Junlin Xiao[1], Rui Li[3], Xiaoying Yang[4], Adam Rushworth[1], and Salman Ijaz[1]

***Abstract*— This work addresses the critical challenge of integrating drones into human-aerial robot interaction by presenting a novel Soft Flexible Aerial Robotics (SFAR) design. SFAR features an innovative low-pressure inflatable airbag structure that replaces traditional rigid frames, enhancing safety by mitigating collision risks with humans and payloads. To control this unconventional aerial platform, we present a control strategy based on a virtual link dynamics model that exploits the drone's unique design. Our contributions include the pioneering design of an aerial robot specifically for Human-Aerial Robot Interaction (HARI), a novel control framework that balances flight performance with passive safety, and the validation of SFAR through real-world experiments, demonstrating its ability to perform at par with traditional rigid-body drones while offering enhanced safety features for seamless and safe integration into human environments.**

I. INTRODUCTION

Human-Robot-Interaction (HRI) is crucial for ensuring that robots can safely, effectively, and ethically integrate into human environments, enhancing our lives through seamless collaboration and assistance. However, HRI research has rarely addressed aerial robots, known as drones, even though they are capable of complex, six-degree-of-freedom maneuverability in three-dimensional spaces and have a wide range of application scenarios. The safety concerns inherent to Human-Aerial Robot Interaction (HARI) are highly challenging; the risks associated with spinning propellers, potential collisions from drones in motion, and the disruptive noise [1], [2] they produce can all lead to serious injuries. Such hazards have the potential to erode public confidence in the safety of these interactions, representing a significant impediment to the broader adoption and collaborative integration of humans and aerial robots in shared environments [3].

To date, researchers have made some strides towards bringing drones into the field of HRI. Hyung-Jin Yoon et al. [4] proposed a socially conscious path-planning framework for drones that takes into account human safety-perceived parameter models and achieves optimal paths with safety guarantees. Similarly, in [5], [6], path planning algorithms centered on human safety perception models are proposed for achieving active human avoidance for mobile robots. Mani Monajjemi et al. attempted to use hand gestures to communicate commands to their drone, which understood the gesture commands using computer vision and responded using lights, facilitating HARI in open environments [7], [8]. From a noise control perspective, Adlakh et al. innovated by including noise metrics in the consideration of trajectory planning to mitigate the impact caused by noise [9]. Additionally, optimizing propeller designs is a well-known approach to improve noise performance.

The concept of incorporating flexible structures into aerial robots has also been investigated. Researchers such as Nguyen et al. [10], Song et al. [11], and Dufour et al. [12] have experimented with creating drones using unconventional materials like inflatable airbags or origami constructions. However, flexible structures present challenges for the controller, as they disrupt the most fundamental assumption in traditional drone controller design—the rigid body assumption [13], [14]. Several studies have endeavored to overcome this challenge [10], [15], [16], [17]. However they also present certain limitations. The static mechanical analysis model struggles with ultra-low-pressure airbags, and the reduces vehicle maneuverability. Additionally, both the finite element and neural network methods are computationally intensive, making real-time high-frequency control challenging [16], [17], [18]. Aerial robots built using these methods often suffer from insufficient propeller protection, poor integration of airbag structures, resulting in a sacrifice of agility, or inadequate control mechanisms that do not allow the full potential of such designs to be realised.

In this work, we present Soft Flexible Aerial Robotics (SFAR), a novel aerial robotic platform featuring a hybrid structural concept that substitutes the conventional rigid frame with a flexible, low-pressure inflatable airbag. The motors, flight controller and payload are all attached to the airbag rather than mechanically connected to each other. This configuration serves as a safeguard, mitigating the risk of injuries to humans and aerial payloads. We proposed a virtual linkage dynamics model and a control strategy for SFAR to handle the flexible drone control challenge. The controller incorporates airbag state estimation, position control, attitude control and the control allocator, utilising the full potential of SFAR.

*This work was supported by Control System Lab at the University of Nottingham, Ningbo, China, and Li Dak Sum Educational Foundation.

[1]Fuhua Jia, Zihao Zheng, Cheng'ao Li, Junlin Xiao, Salman Ijaz, and Adam Rushworth are with the Department of Mechanical, Materials and Manufacturing and Members of Control System Laboratory, University of Nottingham Ningbo China. {fuhua.jia, zihao.zheng, ssyyx19, ssycl4, adam.rushworth, salman.ijaz}@nottingham.edu.cn

[2]Fuhua Jia is also with the Ningbo Innovation Center, Zhejiang University.

[3]Rui Li is with the School of Applied Physics and Electronics, Umea University. ruli0030@student.umu.se

[4]Xiaoying Yang is with the School of Computer Science, University of Nottingham Ningbo China. xiaoying.yang@nottingham.edu.cn

To the best of the authors' knowledge, this is the first aerial robot specifically designed for HARI, which uses a novel, fully encapsulated flexible airbag structure and a controller developed for flexible structure drones to reconcile flight performance with safety. A series of real-world experiments validate the drone's adaptability, showcasing flight capabilities on par with conventional rigid-body drones while offering enhanced protection and flexibility for safe HARI. The core contribution of our work is threefold: (i) a novel aerial robot design based on low-pressure airbag technology to protect humans and airborne payloads from damage in collisions; (ii) a novel virtual linkage dynamic model and control framework for fully flexible aerial robots that integrates flight agility with passive safety; and (iii) performance validation through a series of real-world experiments.

II. PROPOSED FLEXIBLE AERIAL ROBOTICS PLATFORM

A. System Overview

The SFAR platform comprises an inflatable airbag, multiple Propeller Actuator Units (PAUs), an Autonomous Flight Unit (AFU), and payload. The inflatable airbag is equipped with a series of cylindrical holes and cavities, vertically arranged, to accommodate the placement of PAUs and AFU. The surface of the airbag features multiple sets of bosses that are manufactured through an injection moulding process. These bosses serve as attachment points for various other components, allowing for the secure connection and integration of additional elements into the inflatable airbag structure.

Each PAU consists of a motor, propeller, Electrical Speed Controller (ESC), and an Inertial Measurement Unit (IMU) for attitude sensing of the PAU itself. These components are mounted on a rigid carbon fibre frame, which is fastened to the nuts on the surface of the inflatable airbag using screws. The propeller workspace of PAU is positioned within the central region of the holes reserved by the airbag.

The AFU integrates an IMU for attitude sensing, a flight controller responsible for real-time control operations, and a companion computer for executing advanced task functions. The components housed within the AFU are enclosed within a rigid cage that fits snugly within the cavity of the airbag. This cage is connected to the inflatable airbag through a combination of friction and screws. The payload unit is also affixed to the airbag using screws. Both the PAU and AFU adhere to the structural layout of a multi-rotor aerial robot, allowing for versatile configurations such as quad-rotor, hex-rotor, and octo-rotor layouts. The overview of proposed SFAR is depicted in the figure 1.

B. Airbag Frame Structure Design

The airbag in SFAR serves a dual purpose, a main body frame and a collision bumper. The drone's main body frame serves as a support structure for diverse loads and actuators. It is designed to effectively transmit forces and torques, which requires it to be able to maintain a certain level of rigidity and avoid being too soft. On the contrary, the main

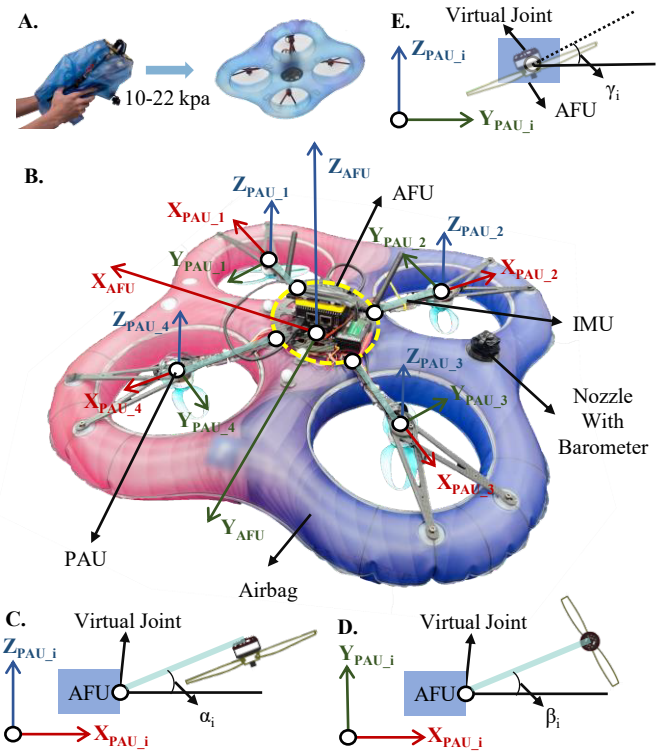

Fig. 1. System overview of proposed SFAR system

frame doubles as a collision bumper, offering a safeguard for the propellers, essential components, and individuals within the drone's vicinity. This collision bumper role necessitates that the airbag be sufficiently soft to mitigate cutting injuries from propellers and absorb collision impact and noise hazard [19]. Balance between stiffness and flexiblilty is an art.

However, this poses a challenge in the design of the airbag structure. Comprising a surface layer, enclosed air, and auxiliary fittings, these elements collectively determine the airbag's properties. The stiffness of the airbag is primarily influenced by the pressure of the air inside and the thickness of the layer. Achieving an optimal balance between airbag stiffness, equipment/personnel protection, and force transmission is therefore crucial to the design process.

Considering the above factors, we chose to use pure TPU as the main material for the construction of the airbag. The airbag consists of several parts of material, the upper and lower layers, and enclosure belts. The upper and lower layers are bonded with nuts, which are used to secure the AFU and PAU as well as other components. The nuts are designed to be tapered in order to increase the welding area between the upper and lower layers. The nut is threaded internally to provide a mounting anchor for the connection.

The enclosure belts use a thicker material than the upper and lower layers to form cylindrical holes and cavities to accommodate the AFU, PAUs, and other components. The use of thicker material limits the inward expansion of the holes and cavities to avoid collision with other parts. The holes for the PAUs have some clearance space to accommodate a degree of independent movement of the PAU components.

Considering the potential risk of rollover, the diameter of the bumper portion of the airbag is approximately 2/3 of the diameter of the propeller in the PAU to ensure that the propeller portion of the PAU will not be easily contacted even in the event of a rollover.

The air pressure of the airbag takes into account the human body's acceptability and is chosen to be between 10-22kpa, which is close to that of a beach volleyball, and can be easily inflated like a ballon without pumps. This setup makes the SFAR similar to Baymax!, an inflatable companion robot from a sci-fi movie that looks much more friendly and relatable.

III. SYSTEM MODELLING

A. Modelling

Due to the inherent softness of the airbag structure, the components exhibit relative mobility with six degrees of freedom. Based on these structural characteristics, we modeled the SFAR system as a virtual linkage-joint model. The model includes the virtual AFU linkage at the center and the virtual PAU linkages surrounding it, each with independent coordinate systems. Initially, the reverse extension of the PAU linkage's X-axis points to the AFU linkage's origin. The PAU linkages are connected to the AFU linkage via a virtual spherical joint with independent resistance and damping coefficients for rotation around three axes. The proposed model is shown in Fig 1. Angles α, β, and γ represent the rotations of the PAU linkage relative to the AFU linkage in the $X-Z$, $X-Y$, and $Y-Z$ planes, respectively, as shown in Fig 1 C, D, and E. Their first and second derivatives correspond to angular velocities and accelerations.

We assume that the rotation angles between the PAU and AFU linkages are minor, staying below 8 degrees. Therefore, the complexities due to the sequence of rotations and the cumulative effects of α, β, and γ can be disregarded. This allows us to simplify the analysis by focusing on the impact of a single angle. However, this angle must still be included in the model, as it cannot be completely neglected. Due to the loose coupling among the linkages, the gyroscopic moments about the x, y, and z axes $[G_{i_x}, G_{i_y}, G_{i_z}]$ for each PAU_i linkage are computed, where i represents any individual PAU. For illustration, a quad-rotor configuration is used, so i ranges from one to four. The PAU coordinate system serves as the reference.

$$\begin{bmatrix} G_{i_x} \\ G_{i_y} \\ G_{i_z} \end{bmatrix} = J_{pf} \cdot \Omega_i \times \begin{bmatrix} \omega_{ix} \\ \omega_{iy} \\ \omega_{iz} \end{bmatrix} \tag{1}$$

where J_{pf} is the moment of inertia of rotating parts including motor rotor and propeller, Ω_i is the rotating velocity of the motor and $[\omega_{ix}, \omega_{iy}, \omega_{iz}]$ is the rotating velocity of the PAU_i linkage in reference to the world coordinate system, as measured by the IMU on the PAU. Translating the force generated by the motor F_{m_i} to the virtual spherical joint:

$$\begin{aligned} F_{m_i} &= F_i + M_{F_i} = F_i + F_{m_i} \cdot L \\ &= F_i + G_{m_{iy}} + J_\alpha \cdot \ddot{\alpha} + K_\alpha \cdot \alpha + C_\alpha \cdot \dot{\alpha} \end{aligned} \tag{2}$$

where L is the distance from the motor of PAU to the virtual spherical joint, J_α is the rotational inertia of the PAU linkage rotating around the virtual spherical joint in the $X-Z$ plane, and $G_{m_{iy}}$ is the component of the gyroscopic moment G_{m_i} around the y-axis. K_α and C_α are the resistance and damping coefficients of the spherical joint as it rotates around the y-axis of the PAU. The torque τ_{m_i} is generated by the motor and should meet the conditions in equation (3):

$$\begin{aligned} \tau_{m_i} &= G_{m_{iz}} + J_\beta \cdot \ddot{\beta} + \tau_i \\ &= G_{m_{iz}} + J_\beta \cdot \ddot{\beta} + K_\beta \cdot \beta + C_\beta \cdot \dot{\beta}. \end{aligned} \tag{3}$$

For the X-axis, take gyroscopic moment into consideration,

$$G_{m_{i_x}} = J_\gamma \cdot \ddot{\gamma} + K_\gamma \cdot \gamma + C_\gamma \cdot \gamma \tag{4}$$

where K_β, K_γ and C_β, C_γ are then the resistance and damping coefficients for the rotation of the spherical joint in the corresponding planes. Modeling with the AFU linkage as the reference coordinate system, the resultant force in the vertical $f_{b,v}$ and horizontal directions $f_{b,h}$, and the resultant moment m_b are:

$$\begin{aligned} f_{b,v} &= \sum F_i \cos\alpha_i \\ f_{b,h} &= \sum F_i \sin\alpha_i \end{aligned} \tag{5}$$

$$\begin{aligned} m_b = \sum -(K_\gamma \cdot \gamma + C_\gamma \cdot \gamma) + (K_\alpha \cdot \alpha + C_\alpha \cdot \dot{\alpha}) \\ + (K_\beta \cdot \beta + C_\beta \cdot \dot{\beta}). \end{aligned} \tag{6}$$

Subsequently, the position model with reference to the earth of the AFU linkage can be obtained:

$$\dot{V}_e = R_b^e \frac{f_{b,v}}{m} + R_b^e \frac{f_{b,h}}{m} - g_e \tag{7}$$

where V_e is the velocity of the AFU link in the Earth coordinate, R_b^e is the transform matrix from the AFU link to the earth frame, g_e is the gravitational constant and m is the total mass of all parts excluding PAUs. The attitude model is obtained by summing all the moments:

$$\tau = J_b \begin{bmatrix} p \\ q \\ r \end{bmatrix} + \begin{bmatrix} p \\ q \\ r \end{bmatrix} \times J_b \begin{bmatrix} p \\ q \\ r \end{bmatrix} \tag{8}$$

where J_b is the moment of inertia of all parts excluding PAUs, τ is the summary of all the moments, p, q, r are the attitude angular velocities of the AFU link. The attitude angle of the AFU link is approximately the same as that in the Earth coordinate system $[\Phi, \Theta, \Psi]$ when the drone is moving in a minor range. Assuming symmetrical component structure except for the PAUs, the model of the system can be obtained.

$$\begin{aligned} \dot{p} &= \frac{1}{I_{xx}} \left[\tau_x + qr\left(I_{yy} - I_{zz}\right)\right] = \ddot{\Phi} \\ \dot{q} &= \frac{1}{I_{yy}} \left[\tau_y + pr\left(I_{zz} - I_{xx}\right)\right] = \ddot{\Theta} \\ \dot{r} &= \frac{1}{I_{zz}} \left[\tau_z + pq\left(I_{xx} - I_{yy}\right)\right] = \ddot{\Psi} \end{aligned} \tag{9}$$

$$\begin{bmatrix}\dot{x}\\ \dot{y}\\ \dot{z}\end{bmatrix} = \frac{f_{b,h}}{m} R_b^e \begin{bmatrix}1\\1\\0\end{bmatrix} + \frac{f_{b,v}}{m} R_b^e \begin{bmatrix}0\\0\\1\end{bmatrix} - g \begin{bmatrix}0\\0\\1\end{bmatrix}. \quad (10)$$

Then the system input can be expressed as: $U = [\tau_x, \tau_y, \tau_z, f_{b,v}, f_{b,h}]$, and they can be mapped to the thrust of each motor and the α, β, γ angles.

B. Parameters Identification

In the SFAR system, all spherical joints share the same parameters, they are $K_\alpha, C_\alpha, K_\beta, C_\beta, K_\gamma$ and C_γ. With the help of IMUs on the AFU and PAUs, the relative virtual joint angles between the AFU and PAUs can be calculated in the following way. Define the transformation rotation $Q_{diff} = Q_{AFU}* \times Q_{PAU}$, where $Q_{AFU}*$ is the conjugate of $Q_{AFU}*$. Denote $Q_{diff} = w + xi + yj + zk$, then, the α, β and γ angle can be obtained.

The angular velocity relationship between them can be obtained directly from the IMU measurement data, and the angular acceleration is a differentiation of the angular velocity.

By analysing the IMU data from the AFU and PAUs, it becomes apparent that the association between these units is notably tenuous. There is no discernible pattern, such as PAUs consistently succeeding AFU, or the reverse. This is further illustrated in Figure 2, which visualizes the unpredictable coupling between AFU and PAU.

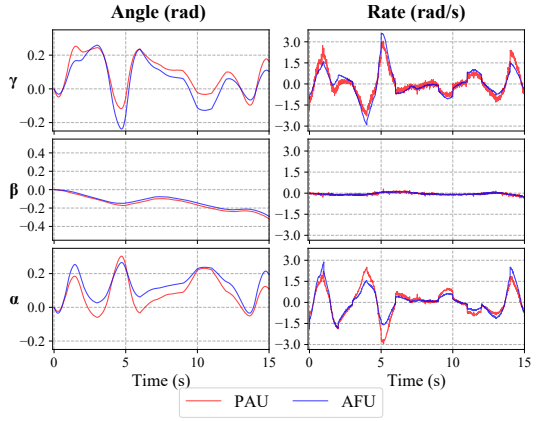

Fig. 2. Measurements obtained after Kalman filtering of IMU data on AFU and PAU in the PAU coordinate system. The air pressure of the airbag was at about 18 kpa during the flight.

Neglecting the sequence of rotations and the cumulative effect of the α, β and γ angles, the resistance and damping parameters can be identified separately in each plane. For the linkage model on each plane, the model can be represented by a second-order differential equation:

$$J\ddot{\theta} + C\dot{\theta} + K\theta = \tau(t) \quad (11)$$

where J is the moment of inertia, $\ddot{\theta}$ is the angular acceleration, C is the damping coefficient, $\dot{\theta}$ is the angular velocity, K is the resistance parameter, and $\tau(t)$ is the external torque applied to the system. The origin of the rotation axis of the PAU linkage is set as the innermost fixed point of its connection with the airbag, as shown in Figure 1, and its moments of inertia around the X,Y and Z axes can be obtained separately using computer-aided design software.

Subsequently, an experiment was designed to estimate the parameters of interest according to Equation (11). First, the SFAR's AFU is secured to a fixed base and a speed command is applied to the PAU's motor. The thrust and torque applied to the PAU are estimated based on the motor and propeller drive models. The angle, angular velocity and angular acceleration information of α, β and γ are recorded.

The least squares method was used to adjust the parameters to be determined in the model until the estimated torque produced by the propeller and the torque calculated from the dynamic equations coincided within these unknown parameters.

The above experimental procedure was tested several times at different air pressure states of SFAR and the relationship between each parameter and air pressure was obtained, as shown in table. I.

Pressure	K_α	C_α	K_β	C_β	K_γ	C_γ
22 kPa	1.2005	0.0289	1.206	0.1956	0.221	0.0001
17 kPa	1.040	0.0317	1.189	0.1920	0.212	0.0001
14 kPa	0.9590	0.0392	1.067	0.1887	0.191	1.4e-4
10 kPa	0.7320	0.0411	0.941	0.1840	0.092	2.9e-4

TABLE I

THE IDENTIFIED DAMPING AND RESISTING COEFFICIENTS OF VIRTUAL JOINTS

IV. CONTROL

The flexible airbag structure loosens the mechanical connections between the components, breaking the rigid body assumption. On the other hand, because SFAR is an underdriven system, the translational and rotational dynamics cannot be fully decoupled for control. Virtual model control, typically utilized in legged robotics, offers an alternative by generating virtual forces and torques from the point of contact to the robot's center of mass, thereby facilitating the derivation of a dynamic model [20]. Inspired by this technique, we propose the following approach. In this section, a control strategy is presented for controlling the aerial robotic platform modeled in section III to track the desired position and achieve control of the flexible structured vehicle.

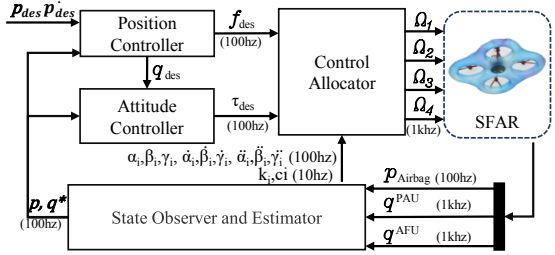

Fig. 3. Control architecture

Figure 3 shows the proposed controller structure. Firstly, using the AFU coordinate as a reference, the position controller calculates the desired combined force and the desired attitude angle. Subsequently, the attitude controller calculates the desired body moment based on the desired attitude angle. The control allocator calculates the force to be generated by the propeller based on the real-time geometric relationship between the AFU and PAUs, obtained from the current airbag state feedback in the PAU coordinate. During the control process, the state observer and estimator process all the AFU and PAU information in real time, calculate their geometric relationship, and update the joint stiffness and damping parameters according to the airbag air pressure.

A. Position Control

The position and tracking control is based on the coordinate system of the AFU. The error between the current position p and the expected position p_{des} obtained by the state estimator is defined as p_{err}. According to the dynamics model in section III, the position of the AFU is affected by the combined force. The integral term with gain k_i is added to the controller to reduce the steady-state error. The required magnitude of the force given by:

$$f_{des} = mR_b^e \left(g + k_p P_{err} + k_i \int P_{err} dt + k_d \dot{P}_{err} \right) \quad (12)$$

where the k_p, k_i and k_d are proportional, integral and derivative terms, respectively, obtained from empirical tuning parameters. Based on f_{des}, the desired AFU attitude angle can be calculated. $\theta_{des} = \arcsin(\frac{F_{x,des}}{F_{z,total}})$, $\phi_{des} = \arcsin(\frac{F_{y,des}}{F_{z,total}})$, where θ_{des} is the desired pitch angle, ϕ_{des} is the desired roll angle, $F_{x,des}$ and $F_{y,des}$ are the horizontal thrust components and $F_{z,total}$ is the total lift.

B. Attitude Control

Attitude control is similar to position control and is performed in the AFU coordinate system. The required torque can be calculated by the attitude controller as $\tau_{des} = K_{pq} q_{err} + K_{iq} \int q_{err} dt + K_{dq} \dot{q_{err}}$, where the q_{err} denotes the error between the current AFU attitude q and the desired AFU attitude q_{des} generated by the position controller, the K_{pq}, K_{iq} and K_{dq} are corresponding coefficients of the attitude controller.

C. Control Allocator

The previously calculated required forces and moments need to be converted into propeller thrust. Firstly, define the control allocator output vector is $U = [u_1, u_2, u_3, u_4]$, according to equations 2-8, then, calculate a forward dynamic output:

$$F^{'} = [f_{b,v}^{'}, f_{b,h}^{'}, \tau_x^{'}, \tau_y^{'}, \tau_z^{'}] \quad (13)$$

Then, define the loss function:

$$Loss = \|(f_{des} - F^{'})\| + \|(\tau_{des} - \tau_x^{'} - \tau_y^{'} - \tau_z^{'})\|. \quad (14)$$

where f_{des} and τ_{des} are desired force and torque from position and altitude controller. Then, with the help of Nonlinear Programming (NLP), desired allocator output can be obtained.

D. State Observer and Estimator

The state observer and estimator play a crucial role in continuously updating the SFAR's pose, attitude, and virtual model parameters in real-time. Pose updates are obtained from external motion capture systems. Attitude, α, β, and γ information are derived from the IMUs of the AFU and PAU, while parameter K and C update are based on the barometer and I.

V. RESULT

In this section, we present the implementation of a prototype aerial robot and experimental evaluation results.

A. Implementation

A quadrotor prototype with the proposed SFAR system has been built, featuring a length and width of 0.60m and a motor-to-motor diagonal distance of 0.38m, as shown in Figure 1. The vehicle comprises one AFU and four PAUs, powered by a four-cell 2200mAh Lipo battery. Each PAU is equipped with a T-Motor 2306 brushless motor, a 50A ESC running blheli-s firmware, and an IMU. Communication between the ESC and AFU uses the Dshot1200 protocol, while the IMU connects to the AFU via the CAN bus.

The AFU includes PX4 FMU flight controller hardware, an onboard computing unit with a Nanopi RK3568, and a hub for power management and CAN bus signal conversion from the PAU. A barometer module with MS5611, installed inside the airbag nozzle, also communicates with the AFU through the CAN bus.

The PX4 FMU handles position and attitude control, while the onboard computing unit manages control allocation and state observation/estimation. These components communicate via the Mavlink port.

B. Experimental results

The experiments are carried out in an indoor test site for robots. In order to showcase the capabilities of proposed SFAR, two different flight tests are executed. The first flight test demonstrated the controller capabilities of the SFAR through trajectory tracking test, which was commanded to track a circle with a radius of 2.0 m and a height of 1.0 m through position and velocity hybrid command, figure 4 shows the trajectory tracking result. It can be seen that SFAR performs well in multi-laps, tracks the desired trajectory well, and has good repeatability.

The second test demonstrated an extreme potential scenario of humans and SFAR being in the same environment. In this scenario, the SFAR involves a human actively hitting the SFAR, and the figure 5 shows the state of the SFAR when the hit occurs. As can be seen from the figure, when the human body actively hits the SFAR, the SFAR undergoes obvious deformation. The SFAR airbag absorbs the impact force well, protecting the human body and the SFAR itself, and the controller stabilizes the SFAR well.

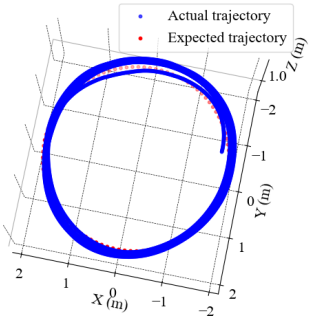

Fig. 4. Trajectory tracking result

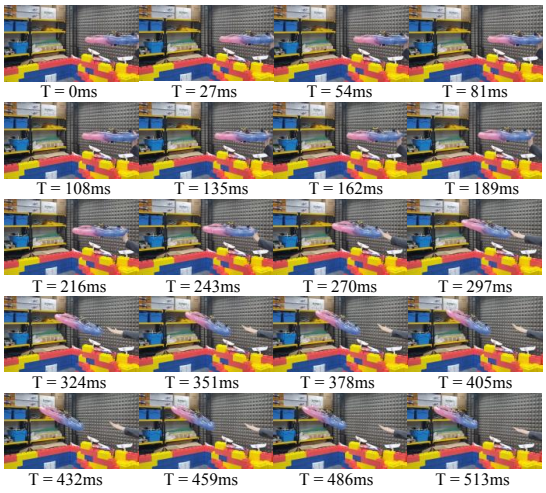

Fig. 5. The response of SFAR after an active impact from human, captured by high-speed camera at 480 fps.

VI. CONCLUSION

In this work, we introduced the SFAR, a novel approach to HARI that promises to enhance the safety and integration of drones in human-centric environments. By replacing the conventional rigid drone frame with a low-pressure inflatable airbag, SFAR mitigates the risks associated with collisions, addressing one of the main safety concerns in HARI. The development of a controller based on virtual linkage dynamics model has proven to be effective in navigating the challenges posed by the drone's flexible structure. Through rigorous real-world experimentation, SFAR has demonstrated its ability to match the flight performance of traditional rigid-body drones, while its innovative design offers a substantial increase in safety for both humans and payloads. Future work should include more detailed modelling and analysis of flexible structures to enable them to take fuller advantage of their benefits. The current design is slightly underutilised in terms of space, with some of the equipment exposed outside the airbag. Furthermore, we plan to apply collision awareness to SFAR, for physical interaction with the environment and other objects.

REFERENCES

[1] M. B. Forrester, "Drone-related injuries treated at emergency departments," *American journal of emergency medicine*, 2019.

[2] J. Callanan, P. Ghassemi, J. DiMartino, M. Dhameliya, C. Stocking, M. Nouh, and S. Chowdhury, "Ergonomic impact of multi-rotor unmanned aerial vehicle noise in warehouse environments," *Journal of Intelligent & Robotic Systems*, vol. 100, pp. 1309–1323, 2020.

[3] U. Acharya, A. Bevins, and B. A. Duncan, "Investigation of human-robot comfort with a small unmanned aerial vehicle compared to a ground robot," in *2017 IEEE/RSJ International Conference on Intelligent Robots and Systems (IROS)*. IEEE, 2017, pp. 2758–2765.

[4] H.-J. Yoon, C. Widdowson, T. Marinho, R. F. Wang, and N. Hovakimyan, "Socially aware path planning for a flying robot in close proximity of humans," *ACM Transactions on Cyber-Physical Systems*, vol. 3, no. 4, pp. 1–24, 2019.

[5] I. Nishitani, T. Matsumura, M. Ozawa, A. Yorozu, and M. Takahashi, "Human-centered x–y–t space path planning for mobile robot in dynamic environments," *Robotics and Autonomous Systems*, vol. 66, pp. 18–26, 2015.

[6] A. Ravankar, A. A. Ravankar, Y. Hoshino, M. Watanabe, and Y. Kobayashi, "Safe mobile robot navigation in human-centered environments using a heat map-based path planner," *Artificial Life and Robotics*, vol. 25, pp. 264–272, 2020.

[7] M. Monajjemi, J. Bruce, S. A. Sadat, J. Wawerla, and R. Vaughan, "Uav, do you see me? establishing mutual attention between an uninstrumented human and an outdoor uav in flight," in *2015 IEEE/RSJ International Conference on Intelligent Robots and Systems (IROS)*. IEEE, 2015, pp. 3614–3620.

[8] M. Monajjemi, S. Mohaimenianpour, and R. Vaughan, "Uav, come to me: End-to-end, multi-scale situated hri with an uninstrumented human and a distant uav," in *2016 IEEE/RSJ International Conference on Intelligent Robots and Systems (IROS)*. IEEE, 2016, pp. 4410–4417.

[9] R. Adlakha, W. Liu, S. Chowdhury, M. Zheng, and M. Nouh, "Integration of acoustic compliance and noise mitigation in path planning for drones in human–robot collaborative environments," *Journal of Vibration and Control*, vol. 29, no. 19-20, pp. 4757–4771, 2023.

[10] P. H. Nguyen, K. Patnaik, S. Mishra, P. Polygerinos, and W. Zhang, "A soft-bodied aerial robot for collision resilience and contact-reactive perching," *Soft Robotics*, 2023.

[11] S. H. Song, H. W. Shon, G. Y. Yeon, and H. R. Choi, "Design and implementation of cloud-like soft drone s-cloud," in *2018 IEEE/RSJ International Conference on Intelligent Robots and Systems (IROS)*. IEEE, 2018, pp. 1–9.

[12] L. Dufour, K. Owen, S. Mintchev, and D. Floreano, "A drone with insect-inspired folding wings," in *2016 IEEE/RSJ International Conference on Intelligent Robots and Systems (IROS)*. Ieee, 2016, pp. 1576–1581.

[13] D. Rus and M. T. Tolley, "Design, fabrication and control of soft robots," *Nature*, vol. 521, no. 7553, pp. 467–475, 2015.

[14] C. Lee, M. Kim, Y. J. Kim, N. Hong, S. Ryu, H. J. Kim, and S. Kim, "Soft robot review," *International Journal of Control, Automation and Systems*, vol. 15, pp. 3–15, 2017.

[15] F. Ruiz, B. C. Arrue, and A. Ollero, "Sophie: Soft and flexible aerial vehicle for physical interaction with the environment," *IEEE Robotics and Automation Letters*, vol. 7, no. 4, pp. 11 086–11 093, 2022.

[16] M. Ryll and R. K. Katzschmann, "Smors: A soft multirotor uav for multimodal locomotion and robust interaction," in *2022 International Conference on Robotics and Automation (ICRA)*. IEEE, 2022, pp. 2010–2016.

[17] S. Bennaceur and N. Azouz, "Modelling and control of a quadrotor with flexible arms," *Alexandria Engineering Journal*, vol. 65, pp. 209–231, 2023.

[18] T. Cui, X. Yang, F. Jia, J. Jin, Y. Ye, and R. Bai, "Mobile robot sequential decision making using a deep reinforcement learning hyper-heuristic approach," *Expert Systems with Applications*, p. 124959, 2024.

[19] R. Weitschat, J. Vogel, S. Lantermann, and H. Höppner, "End-effector airbags to accelerate human-robot collaboration," in *2017 IEEE international conference on robotics and automation (ICRA)*. IEEE, 2017, pp. 2279–2284.

[20] J. Pratt, P. Dilworth, and G. Pratt, "Virtual model control of a bipedal walking robot," in *Proceedings of international conference on robotics and automation*, vol. 1. IEEE, 1997, pp. 193–198.